
Article:
Ashton, Rhys, Silver, Callum, Bird, Toby et al. (3 more authors) (2023) Enhancing the repeatability and sensitivity of low-cost PCB, pH-sensitive field-effect transistors. Biosensors & bioelectronics. 115150. ISSN: 0956-5663

https://doi.org/10.1016/j.bios.2023.115150

Biosensors and Bioelectronics 227 (2023) 115150

Contents lists available at ScienceDirect

Biosensors and Bioelectronics

journal homepage: www.elsevier.com/locate/bios

Enhancing the repeatability and sensitivity of low-cost PCB, pH-sensitive field-effect transistors

Rhys Ashton *, Callum D. Silver, Toby W. Bird, Ben Coulson [1], Andrew Pratt, Steven Johnson **

School of Physics, Engineering & Technology, University of York, York, YO10 5DD, UK

ARTICLE INFO

Keywords:
pH sensor
PCB
Iridium oxide
Discrete ISFET
Biosensors
β-Lactamase

ABSTRACT

Discrete, extended gate pH-sensitive field-effect transistors (dEGFETs) fabricated on printed circuit boards (PCBs) are a low-cost, simple to manufacture analytical technology that can be applied to a wide range of applications. Electrodeposited iridium oxide (IrOx) films have emerged as promising pH-sensitive layers owing to their theoretically high pH sensitivity and facile deposition, but typically exhibit low pH sensitivity or lack reproducibility. Moreover, to date, a combined IrOx and dEGFET PCB system has not yet been realised. In this study, we demonstrate a dEGFET pH sensor based on an extended gate manufactured on PCB that is rendered pH sensitive through an electrodeposited IrOx film, which can reliably and repeatably display beyond-Nernstian pH response. Using a combination of complementary surface analysis techniques, we show that the high pH sensitivity and repeatability of the dEGFETs are dependent on both the chemical composition and critically the uniformity of the IrOx film. The IrOx film uniformity can be enhanced through electrochemical polishing of the extended gate electrode prior to electrodeposition, leading to dEGFETs that exhibit a median pH sensitivity of 70.7 $\pm$ 5 mV/pH (n = 56) compared to only 31.3 $\pm$ 14 mV/pH (n = 31) for IrOx electrodeposited on non-polished PCB electrodes. Finally, we demonstrate the applicability of these devices by demonstrating the detection and quantification of ampicillin due to β-Lactamase enzyme activity, thus laying the foundation for cheap and ubiquitous sensors which can be applied to a range of global challenges across healthcare and environmental monitoring.

1. Introduction

Technologies capable of quantifying changes in pH are used across analytical chemistry, environmental monitoring and bioscience. For example, the activity of many important enzymes, such as nucleic acid polymerases and β-lactamase enzymes, is mediated by proton-transfer reactions resulting in acidification of the local environment in low-buffer capacity solutions. pH sensors capable of quantifying this change in pH can be exploited to indirectly detect and quantify enzymatic activity. For example, ion-sensitive field-effect transistors (ISFETs) with H^+ sensitive membranes, such as those used on the commercial IonTorrent (Rothberg et al., 2011) and DNAe (Toumazou et al., 2013) next-generation sequencing (NGS) platforms, have been widely used to detect and quantify polymerase-mediated DNA synthesis (Salm et al., 2014).

ISFETs used in NGS systems are typically realised as bespoke integrated circuits (ICs) manufactured using complementary metal oxide semiconductor (CMOS) technology. This enables the fabrication of high-density ISFET arrays to meet the highly multiplexed detection requirements of NGS. However, there are numerous applications for pH measurement where multiplexing at this scale is not required, for example, testing susceptibility to β-lactam antibiotics. Here the priorities are speed, sensitivity, reproducibility and critically, cost.

Low-cost, single device ISFETs can be realised using commercial, discrete FETs coupled to an extended gate electrode that is rendered pH sensitive. Such extended gate, discrete ISFETs (dEGFETs) (Chi et al., 2000) provide physical separation of the FET from the pH-sensitive layer, simplifying packaging and encapsulation. Moreover, in contrast to CMOS-based ISFET ICs, the dEGFET structure is compatible with a wide range of substrates and sensing layers, which can be selected to

* Corresponding author.
** Corresponding author.
E-mail addresses: rhys.ashton@york.ac.uk (R. Ashton), callum.silver@york.ac.uk (C.D. Silver), toby.bird@york.ac.uk (T.W. Bird), coulsonba@gmail.com (B. Coulson), andrew.pratt@york.ac.uk (A. Pratt), steven.johnson@york.ac.uk (S. Johnson).
[1] Present address: School of Chemistry, Cardiff University, Park Place, Cardiff, CF23 5 EF, UK.

https://doi.org/10.1016/j.bios.2023.115150
Received 20 December 2022; Received in revised form 30 January 2023; Accepted 12 February 2023
Available online 16 February 2023

balance device cost and ease of manufacture with high pH sensitivity and biological compatibility.

While a range of substrate materials have been explored (Prodromakis et al., 2011a; Yin et al., 2000; Hung et al., 2014; Cho and Lim, 2018) printed circuit boards (PCBs) have emerged as a highly compelling choice for the fabrication of extended gate electrodes. PCBs are widely used across the consumer electronics industry. As a result, these materials are readily available at low cost and there exists multiple established approaches for manufacturing patterned PCB substrates at scale. Moreover, recent research has demonstrated the possibility of integrating microfluidic channels within PCBs, enabling the realisation of Lab on Chip (LoC) devices that combine sensing and fluidics on the same substrate (Kaisti et al., 2016; Moschou et al., 2015).

Despite these advantages, the copper electrodes used in PCBs are inherently weakly pH-sensitive (Yang et al., 2012; Zaman et al., 2011) requiring additional fabrication stages for integration of a pH-sensitive coating. The pH sensitivity of these surface coatings is described by the Nernst equation (eq. (1)) where, E is the electrode potential, E_0 the standard electrode potential and R, T and F are standard constants. As can be seen from eq. (1), under constant conditions, the magnitude of the pH response is determined by the stoichiometric coefficient of hydrogen ion activity (h) and the number of electrons transferred during the redox reaction (n). For many pH-sensitive coatings, h and n are equal (Huang et al., 2011) leading to a maximum sensitivity of 59.2 mV/pH; the Nernstian limit. In practice however, the response of pH sensing layers observed experimentally is typically lower than the Nernstian limit, including those employed on PCB dEGFETs which exhibit a response significantly below this limit (Prodromakis et al., 2011b; Trantidou et al., 2013).

$$E = E_0 + \frac{h}{n}\frac{2.303RT}{F}pH \tag{1}$$

Recent attention has focused on a range of metal oxide sensing layers (Manjakkal et al., 2020), such as hydrated iridium oxide (IrOx), that have the potential to offer enhanced pH sensitivity. The increased sensitivity originates from redox reactions between specific complexes of Ir^{3+} and Ir^{4+} oxidation states (eq. (2)) (Olthuis et al., 1990). Eq. (2) shows an imbalance between h and n, resulting in an enhanced theoretical pH sensitivity when substituted into the Nernst equation (eq. (3)).

$$2Ir(OH)_2O^- + H_2O \rightleftharpoons Ir_2O(OH)_3O_3^{3-} + 3H^+ + 2e^- \tag{2}$$

$$E = E_0 + \frac{3}{2}\frac{2.303RT}{F}pH = 88.8\ mV\Big/pH \tag{3}$$

It should be noted that while a change in Ir oxidation state is universally agreed to contribute to the enhanced pH sensitivity, consensus has yet to be reached around the mechanism described in eq. (2) (Steegstra et al., 2013; Hillman et al., 2011). Moreover, the oxidation state of the IrOx layer is linked to the degree of hydration within the film. Hydrated IrOx films produced by low cost and simple to implement electrodeposition processes are favourable for producing highly pH-sensitive films (Olthuis et al., 1990; Burke and Whelan, 1984; Kim and Yang, 2014).

IrOx films have been explored for use as pH sensing electrodes (Marzouk, 2003; Zea et al., 2019; Gowers et al., 2019) in which the open circuit potential (OCP) of an IrOx coated electrode is a measure of pH. In such devices, pH sensitivities of up to 79 mV/pH (Elsen et al., 2009) have been obtained albeit with slow response times (≈10 s). While ISFET and dEGFET devices provide faster response times to characterise rapid kinetics, ISFETs with IrOx pH-sensitive films have yet to be demonstrated that approach the theoretical maximum pH sensitivity (Kim et al., 2003; Hendrikse et al., 1997). Moreover, to the best of our knowledge, there exists only a single study that has explored the pH sensitivity of IrOx films deposited on PCB-based electrodes (Anastasova et al., 2018). While this device confirmed the possibility of high pH sensitives (73 mV/pH), the electrodes required both an Au finish during PCB fabrication and an additional Au nanoparticle electrodeposition prior to IrOx film deposition.

In this work, we demonstrate for the first time pH sensitivity beyond the traditional Nernstian limit using a dEGFET in which the extended gate was fabricated on PCB and modified by electrodeposition of IrOx, showcasing truly low-cost and high performance dEGFETs (median response of 70.7 mV/pH). Moreover, we demonstrate very low device-to-device variability (SD ± 5 mV/pH) in the pH response which is critical for future translation and widespread adoption of this technology. A facile approach for electrode treatment prior to electrodeposition is essential for both increased pH sensitivity and significantly enhanced reproducibility. Using a range of complementary surface analysis techniques, we show that this high pH sensitivity and repeatability are related to the increased uniformity of IrOx films electrodeposited on PCB electrodes that have undergone electrochemical polishing of the Cu electrode prior to electrodeposition. Finally, we demonstrate the application of the IrOx, PCB-based dEGFET through detection and quantification of enzymatic activity via turnover of β-lactamase antibiotics.

2. Materials and methods

2.1. Chemicals and reagents

0.05 M potassium phosphate (KPI) buffers were prepared using phosphate mono/di basic (Sigma Aldrich, UK). These ranged from pH 6 to 8 at intervals of 0.5, with pH confirmed to be within 0.01 pH using a commercial Mettler Toledo pH meter (FiveEasy and Inlab Expert Pro). Citric acid was produced at 10% w/v from a powder (Sigma Aldrich, UK). Ultrapure water (18.2 MΩ/cm, MilliQ) was used for preparation of all aqueous solutions.

Stock solutions of a β-Lactamase Blend (Sigma Aldrich, UK, L7920) of recombinant enzymes expressed in *Escherichia coli* were prepared by dissolving in 50 mM KPI (pH7) buffer, stored at −20 °C, and used without further dilution. Each aliquot contained 40–70 IU β-lactamase I and 6–10 IU β-lactamase II. Solutions of anhydrous ampicillin (Sigma Aldrich, UK, 271861) were made in 0.5 mM KPI (pH 7) buffer with 50 mM potassium sulphate (Sigma Aldrich, UK).

2.2. Measurement and characterisation

Scanning electron microscopy (SEM) was performed using a JEOL 7800F Prime scanning electron microscope. The instrument includes an Oxford Instruments AZtec Energy-dispersive X-ray spectroscopy (EDX) system containing 2 detectors. EDX maps were collected using a beam energy of 5 keV with fixed acquisition settings (× 3, 300 magnification, frame duration of 40 s, frame count of 10, and 50 μs dwell time). EDX analysis was performed using the Oxford Instruments AZtec software while particle analysis of SEM images was performed with ImageJ using the Otsu intensity threshold algorithm (Otsu, 1979) to quantify nanoparticle size and density.

Atomic Force Microscope (AFM) images were obtained using a Bruker Bioscope Resolve in tapping mode with an RTESPA300 tip. Surface roughness analysis was performed using ImageJ.

X-ray photoelectron spectroscopy (XPS) experiments were performed in an ultrahigh vacuum system with a base pressure of $< 3 \times 10^{-10}$ mbar, using a monochromated Al Kα source at 1486.6 eV (Omicron XM 1000) and a power of 220 W. An aperture diameter of 6 mm was used with the sample normal at 45° to both the X-ray source and the entrance optics of the hemispherical energy analyzer (Omicron EA 125). XPS spectra were referenced to adventitious carbon peak at 284.8 eV. Binding energies were attributed using the NIST database (National Institute of Standards and Technology, 2000) and values for Ir oxidation states were informed by literature (Pfeifer et al., 2016; Freakley et al., 2017). Peak deconvolution and fitting were carried out manually using XPSPEAK4.1 software. Subsequently, atomic % for elements and species

were obtained using the integral of the respective spectra using OriginPro peak find against a Shirley background, and applying the appropriate correction factors (Wagner et al., 1981).

Cyclic voltammetry (CV) was performed using an SP-300 Biologic potentiostat in a three-electrode configuration consisting of a Cu PCB working electrode, a Pt wire counter electrode and a Ag/AgCl/Saturated KCL double junction reference electrode. KPI and the Iridium Oxalate deposition solution with and without Iridium were used as electrolytes. The potential was cycled between −0.5 V and 0.8 V vs. Ag/AgCl at a scan rate of 100 mV/s. CV peak analysis was performed using Origin Pro with a linear baseline to the non-Faradaic background current.

2.3. PCB sensors

The extended gate electrodes were designed using Eagle software and manufactured through a commercial PCB supplier (Fig. 1a) (Eurocircuits, Belgium). The Cu electrodes were supplied without surface finish on an FR4 substrate (Technolam GmbH, NP-155FR). The Cu layer thickness was measured to be 30 ± 1.7 μm (Bruker DektakXT; n = 6). Prior to use, all electrodes were submerged in 10% citric acid (Sigma Aldrich, GB) for 15 min to remove oxide from the contact pads. Where required, electrodes were subsequently electropolished in a 60% dilution of stock 85% Phosphoric Acid (Fluorochem, UK) by applying 1.4 V between the Cu electrode and Pt wire counter for 6 min (Awad et al., 2010).

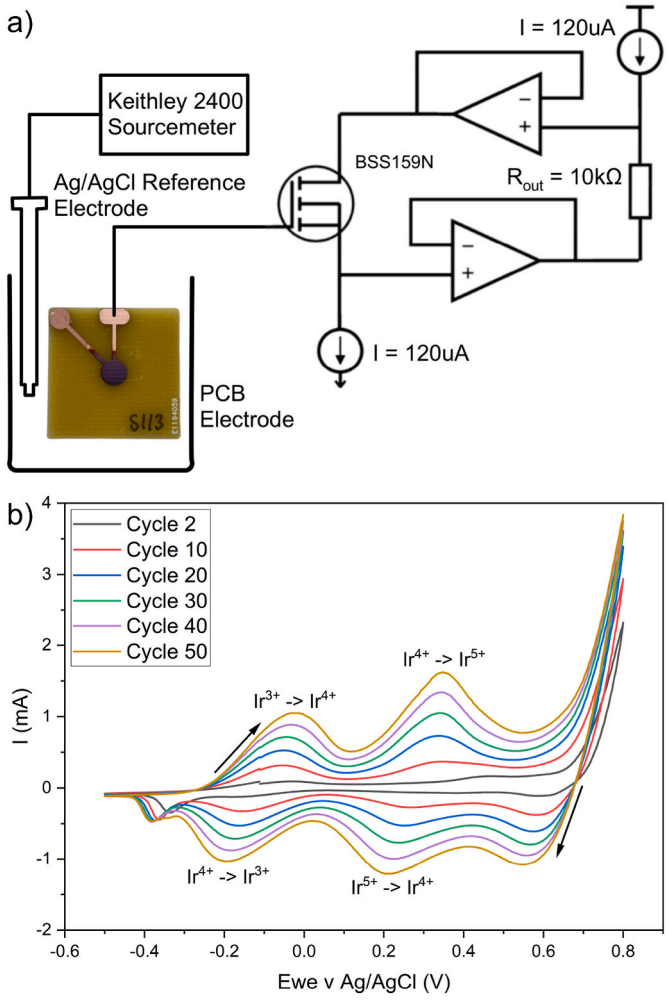

Fig. 1. a) System diagram including biasing and readout circuitry and the extended gate PCB electrode. Adapted with permission from (Kaisti et al., 2016). Copyright 2022 American Chemical Society. b) Cyclic voltammetry during electrodeposition of an IrOx film on the extended gate Cu PCB electrode, with Ir reduction/oxidation peaks between oxidation states indicated. The redox peaks have been attributed using CVs taken before and after IrOx deposition in different electrolytes and informed by literature. Additional attributed peaks are indicated in Fig. 2d) and further detail including supporting CVs are shown in SI S1).

2.4. ISFET biasing and readout circuitry

The PCB-dEGFET pH sensor was connected to a biasing and readout circuit, shown in Fig. 1a), that was fabricated in-house based on a previous design (Kaisti et al., 2016). The gate voltage is the sum of the voltage on the double junction Ag/AgCl/Saturated KCL bias electrode (ALS, Japan) and the potential difference at the electrode/electrolyte interface; $V_g = V_{bias} + V_{interface}$. V_{bias} was fixed for each transistor and selected to bias the device into its linear triode region such that a change in $V_{interface}$ will lead to a linear change in V_g. The optimum bias voltage was identified by sweeping V_{bias} between −0.6 V and −1.4 V. For a more detailed discussion of the mode of operation of ISFET sensors, we refer the reader to the relevant literature (Bergveld, 2003; Yates et al., 1974).

The readout circuitry employs a constant-voltage, constant-current (CVCC) configuration, such that the source-drain current through the transistor is fixed at 120 μA. R_{out}, in tandem with a second constant current source, dictates the source-drain voltage which here was fixed at 1.2 V. A change in $V_{interface}$ and thus V_g, results is a change in source voltage (V_s) which is mirrored across the operational amplifiers. The electrical isolation enabled by the high input impedance of the operational amplifiers prevents loading of the transistor and unwanted changes to the transistor biasing. A Picolog 1216 12-bit DAC (Pico Technology, UK) was used to digitise the resulting output signal measured with respect to ground.

All components are discrete surface-mount including the BSS159N depletion mode n-type MOSFET, selected due to its low cost and low gate leakage current. LM334M/NOPB was used as a current regulator, LT3045EMSE#PBF-ND as a voltage regulator and LTC6079IGN#PBF as a dual operational amplifier package. DC power was supplied by an external voltage source (GW Instek GPS-4303) while the bias voltage was supplied to the reference electrode using a Keithley 2400 Sourcemeter.

2.5. Electrochemically deposited iridium oxide

A three-electrode cell consisting of a Cu PCB working electrode, Pt wire counter and Ag/AgCl reference electrode were used for the IrOx electrodeposition. Electrodes were coated with an IrOx film by electrodeposition from an iridium oxalate solution, as described in (Yamanaka, 1989). Briefly, (1) Iridium chloride hydrate ($IrCl_4 \cdot H_2O$: 0.15 g) (Alfa Aesar, UK) was dissolved in 100 mL of water by magnetic stirring for 30 min (2) 1 mL of aqueous hydrogen peroxide solution (H_2O_2: 30% wt.) (Sigma Aldrich, UK) was added and stirred for 10 min (3) Oxalic acid ($(COOH)_2 \cdot 2H_2O$: 0.5 g) (Sigma Aldrich, UK) was added and stirred for 10 min (4) Anhydrous potassium carbonate (Sigma Aldrich, UK) was finally added to adjust the solution pH to 10.5. (5) The resulting solution was left to stabilise for 3 days, after which it adopts a dark blue colour.

Electrodeposition was performed using cyclic voltammetry (Biologic SP-3000 potentiostat) allowing the growth of the IrOx film to be monitored (Fig. 1b)). All sensors underwent 50 potential cycles between 0.8 and −0.5 V vs. Ag/AgCl at 100 mV/s and at room temperature. We note, the resulting IrOx layers were observed to be mechanically unstable below 20 potential cycles.

2.6. β-Lactamase measurements

ISFET sensors were exposed to solutions of different ampicillin concentrations (up to 200 μg/mL) in KPI buffer. The initial output voltage of the dEGFET for each solution was recorded to provide a baseline measurement. 100 μL of the aliquoted β-Lactamase blend was

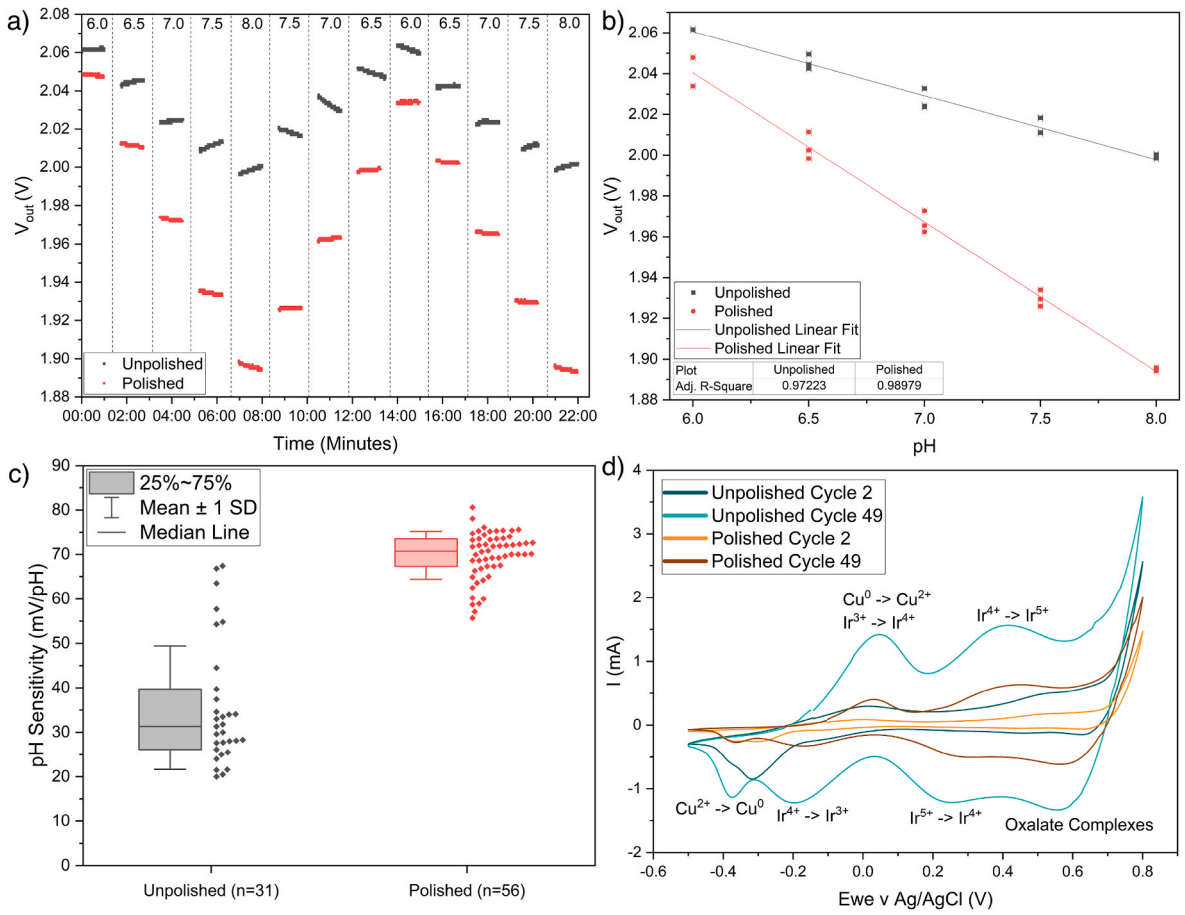

Fig. 2. a) dEGFET output voltage using IrOx pH sensitive layer electrodeposited on unpolished and polished PCB electrodes. The solution pH is indicated at the top of the graph for each 60 s data collection window. b) Mean average voltage of each plateau plotted against pH. c) pH sensitivity of unpolished and polished sensors. Box shows median value and 25th and 75th percentiles, while whiskers show ±1 SD from the mean. All points are displayed to the side as a half violin plot. d) CV during deposition of IrOx films on both unpolished and polished sensors.

subsequently added to 15 mL of the ampicillin solution and allowed to incubate for 45 min before the output voltage was again measured. The voltage change, alongside measured pH sensitivity of the sensor was combined to quantify the corresponding change in pH. Control experiments followed the same procedure, except with no ampicillin in the KPI buffer. All measurements were performed at room temperature.

3. Results and discussion

3.1. pH sensitivity of IrOx coated PCB electrodes: unpolished vs. polished

The pH-sensitive dEGFET platform is shown in Fig. 1a). Each device consists of a 5 mm diameter Cu electrode coated with an electrodeposited IrOx film and fabricated on a PCB substrate. This pH-sensitive electrode is connected to the gate electrode of a discrete MOSFET mounted on a separate PCB that includes the associated bias and readout circuitry. The pH sensitivity of the IrOx coated electrodes was determined by exposing the IrOx surface to a range of 50 mM KPI buffer solutions of differing pH. Fig. 2a) shows the output voltage of an unpolished, IrOx-coated electrode as a function of solution pH while Fig. 2b) shows the mean voltage recorded at each pH. Here, unpolished refers to those electrodes which were only cleaned by 15 min immersion in citric acid prior to electrodeposition. While the dEGFET clearly showed reversible changes to solution pH, the pH sensitivity, defined as the gradient of the straight line fit to the data in Fig. 2b), was only 31.4 mV/pH; far below the theoretical limit of 88.8 mV/pH. Moreover, the pH sensitivity of these unpolished electrodes was highly variable, as shown in Fig. 2c), with a median value of 31.3 mV/pH (n = 31 electrodes) and a standard deviation of 14 mV/pH.

In contrast, Fig. 2a) and b) also show the shift in dEGFET output voltage using Cu electrodes that were electropolished prior to IrOx electrodeposition. Here, the dEGFET displayed a pH sensitivity of 73.3 mV/pH; well beyond the traditional Nernstian limit. Moreover, electropolishing of the electrodes markedly improved the reproducibility of the pH sensitivity. Specifically, from measurements of a large number (n = 56) of nominally identical, polished electrodes we observed a median pH sensitivity of 70.7 mV/pH and a standard deviation of only 5 mV/pH. The pH sensitivity and repeatability of our electrodes are compared against other potentiometric pH sensors fabricated using PCB substrates and IrOx sensing layers in SI S2) Tables 1 and 2 respectively.

To better understand the origins of the high pH sensitivity and reproducibility of polished Cu electrodes, we conducted a detailed study of the physical, chemical and electrochemical characteristics of the IrOx films electrodeposited on unpolished and polished electrodes.

3.2. Electrochemical analysis of IrOx deposition

Fig. 2d) shows typical cyclic voltammograms recorded during electrodeposition of IrOx on both unpolished and polished Cu electrodes for the first and final full voltage cycles. All curves are representative (raw data for 3 independent electrodes shown in SI S3)).

Differences between the polished and unpolished samples are observed in the first full voltage cycle of the CV (Fig. 2d) cycle 2). Specifically, the non-faradaic current for the unpolished electrodes is

roughly twice that observed for electropolished electrodes. This component is associated with the capacitance of the electrode-electrolyte interface where the larger capacitance of the unpolished electrode can be ascribed to either an increased surface roughness, leading to a larger apparent electrode surface area, or the existence of a thin contamination layer at the electrode surface. Closer inspection of the voltammograms indicates a reduction peak around −0.3 V vs Ag/AgCl that is much larger on the unpolished electrodes. From CV measurements designed to isolate redox activity of the surface and electrolyte components (SI S2)) and supported by literature (Giri and Sarkar, 2016; Naseer and Khan, 2009; Shaikh et al., 2011), we ascribe this to the reduction of Cu^{2+} to Cu^{0}. We believe this is related to a native oxide present at the surface of unpolished electrodes (this is further supported by chemical analysis, see Sections 3.4 & 3.5).

As the number of voltage cycles progresses, reduction and oxidation peaks associated with redox active groups within the IrOx film emerge. Specifically, oxidation peaks associated with the Ir^{3+} - Ir^{4+} and Ir^{4+} - Ir^{5+} transitions are observed at 0.05 V and 0.41 V vs Ag/AgCl respectively. The cathodic charge storage capacity (CSC_c), which correlates with the density of redox active groups in the IrOx film, can be calculated from the time integral of the CV cathodic current coupled with the electrode area (0.785 cm^2) (Meyer et al., 2001). At the end of deposition, shown in Fig. 2d) and SI S3), we observed a significantly higher CSC_c and thus increased density of redox active groups on the unpolished electrodes (13.51 ± 2.03 mC/cm^2) than on those that had been electrochemically polished (5.13 ± 0.46 mC/cm^2). As the high pH-sensitivity of IrOx films is associated with this redox activity, one might naturally assume that those sensors with the greater density of redox active groups would inherently provide higher pH sensitivity. This is contrary to what we observe in this work, where the polished electrodes associated with a lower density of redox active groups display the higher sensitivity.

3.3. Physical characterisation via SEM & AFM

SEM and AFM analysis were performed to characterise the electrode surface morphology, comparing differences between the electrodes before and after electropolishing, and following IrOx deposition. The difference in surface roughness between unpolished and polished Cu electrodes can be seen clearly in the representative SEM images of Fig. 3a) and 3b) and in the AFM images of SI S4a) and SI S4b) respectively. The surface of the unpolished Cu electrode was seen to be covered in a network of deep grooves (Fig. 3a) and SI S4a)) and exhibited an RMS surface roughness of 275 ± 36 nm. After electropolishing, the grooves were seen to have significantly reduced in depth leading to a surface that resembled flat terraces, possibly polycrystalline domains, that extend over areas of 10's μm^2 (Fig. 3b) & SI S4b)). Accordingly, the surface roughness also reduced significantly to 62.7 ± 23 nm. Here, the mean RMS roughness was calculated from AFM images of 4, nominally identical electrodes with each surface being imaged at 3, different 50 μm^2 scan regions (raw data SI S4c)).

SEM images of the IrOx film electrodeposited on the Cu electrodes reveal individual nanoparticles and clusters of nanoparticles that decorate the surface of both unpolished (Fig. 3c)) and polished electrodes (Fig. 3d)). The diameters of the individual particles are around 100–200 nm while the nanoparticle clusters range between 1 and 20 μm. It was not possible to obtain AFM images of the surface of the IrOx films as the surface roughness was larger the AFM dynamic range (>10 μm).

While nanoparticles were observed following IrOx electrodeposition on both unpolished and polished electrodes, particle analysis reveals marked differences in the average nanoparticle diameter (Fig. 3e)) and surface coverage (shown in SI S6)). On average, the nanoparticle clusters are around 3 × larger in diameter on unpolished compared to polished electrodes and cover a larger area of the unpolished electrode surfaces. The higher surface coverage of IrOx nanoparticle clusters is consistent with CV analysis of the electrodeposition process that revealed a greater density (2.6 ×) of redox active groups in IrOx films on unpolished sensors. This data suggests that the high surface roughness and surface contamination associated with unpolished electrodes leads to the preferential deposition of IrOx nanoparticle clusters, likely through field enhancement and local suppression of interfacial charge transport, both

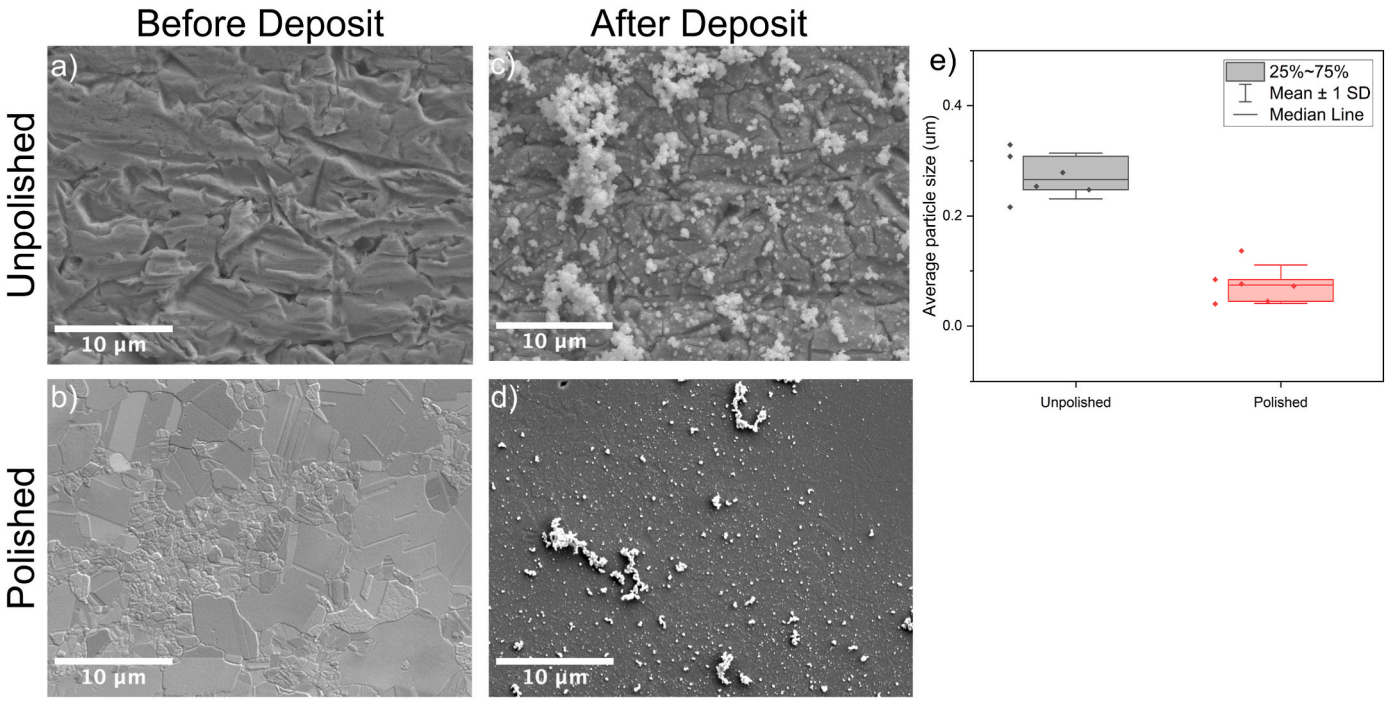

Fig. 3. SEM images of a) unpolished and b) electrochemically polished Cu electrodes on PCB before deposition of IrOx. SEM images of the IrOx film electrodeposited on c) unpolished and d) polished Cu electrodes. e) Analysis of average nanoparticle diameter following electrodeposition of IrOx on polished and unpolished Cu electrodes. Data extracted from analysis of SEM images of 6 unpolished and 6 polished sensors. Box shows median value and 25th and 75th percentiles, while whiskers show ±1 SD from the mean. Higher magnification images are shown in SI S5).

of which are reduced following electrochemical polishing of the Cu electrode surface prior to electrodeposition.

3.4. Energy-dispersive X-ray spectroscopy (EDX)

Having confirmed the physical characteristics of the electrodes and associated IrOx films, we next employed EDX to examine the chemical composition of IrOx films electrodeposited on both unpolished and polished electrodes. EDX analysis of the Cu electrodes prior to IrOx deposition confirms only Cu, C and O are present. Fig. 4a) compares the elemental ratios between unpolished and polished Cu electrodes prior to IrOx deposition. Polished electrodes show consistently lower C and O contamination (2% combined across the complete surface compared to 7.9% on unpolished electrodes). Notably, oxygen contamination is 4.5 × greater in unpolished devices. This is in agreement with previously presented CV deposition data for unpolished electrodes where we observed a redox peak ascribed to reduction of CuO and a higher interfacial capacitance associated with a thin native oxide at the electrode surface.

The spatial distribution of C and O contamination on blank Cu electrodes was observed from EDX maps. Unpolished surfaces (SI S7a)) show broad background contamination (≈ 5% C) across the surface, interestingly, we also observe many regions of elevated contamination (often comprising > 30% C & > 5% O). Such areas of high contamination will locally impede the electrodeposition process and thus reduce the uniformity of the resulting IrOx film. In contrast, elemental maps of polished electrodes (SI S7b)) show no areas of elevated contamination and background contamination is much reduced (< 0.5% combined C and O). There is also a reduction in the standard deviation of elemental composition across the surface, suggesting a more consistent and uniform chemical composition of the polished electrode surface.

Fig. 4b) shows EDX analysis of the IrOx films electrodeposited on both polished and unpolished electrodes and confirms the added presence of Ir, and an increase in O concentration. Although Ir and Cu are shown to have broad coverage across both unpolished and polished electrodes, the ratio of Ir to Cu is lower on the polished electrodes (0.82 : 1 in contrast to 2.34 : 1 on unpolished electrode). Moreover, EDX images (shown in SI S7c) & SI S7d)) confirm the nanoparticles and clusters observed in the SEM images (Fig. 3c) and d)) contain Ir. These findings are in agreement with our analysis of CV and SEM data that revealed greater surface coverage of the unpolished electrode surface with Ir containing nanoparticle clusters.

3.5. X-ray photoelectron spectroscopy (XPS)

EDX provides high throughput and quantifiable chemical analysis, however the incident electron beam penetrates beyond the surface of the sample, to a depth much greater than the IrOx layer thickness. As a result, the EDX signal associated with IrOx deposited samples contains a contribution from the bulk Cu substrate. We thus exploited the low analytical depth (typically around 5–10 nm) associated with XPS to better understand the chemical composition of the electrodeposited IrOx film. Complete XPS spectra for uncoated Cu electrodes (SI S8)) and for IrOx films deposited on both unpolished and polished electrodes (SI S9)) can be found in the SI.

As with EDX of the blank unpolished Cu electrodes (SI S10)), XPS revealed a higher combined atomic % of carbon and oxygen contaminants adsorbed on the surface. Deconvolution of the O 1s region, indicates that 66% of the oxygen on the surface of unpolished electrodes is associated with a surface oxide compared to only 48% in polished electrodes. Differences in the ratio of copper species also indicate the presence of an oxide layer on the surface of unpolished electrodes compared to the polished electrodes. Specifically, for unpolished electrodes (Fig. 5a)), the bulk Cu^0 signal accounts for 59.8% of the total copper, the remaining (40.2%) being Cu^{2+} associated with cupric oxide (CuO). This contrasts with the polished electrodes (Fig. 5b) in which the oxide is removed by the process of electropolishing, leading to a reduction in the Cu^{2+} species to 20.6%. The higher fraction of surface Cu in its bulk state (79.4%) is better suited to uniform electrodeposition of IrOx layers.

XPS spectra (SI S10)) of IrOx films deposited on unpolished electrodes also show persistently elevated levels of contamination compared to films deposited on electropolished Cu electrodes. Moreover, Cu, likely associated with the underlying Cu electrodes, is also observed in XPS spectra of IrOx coated unpolished electrodes. The thickness of IrOx layers electrodeposited by cyclic voltammetry has been measured at around 40 nm (Elsen et al., 2009; Hu et al., 2009). This is much larger than the analytical depth of XPS suggesting that the IrOx layer is not uniform, leading to regions of exposed bulk Cu surface.

We note, given the accepted dependence between pH sensitivity of IrOx films and the Ir oxidation state (Steegstra and Ahlberg, 2012), the increased pH sensitivity observed in polished samples could in part be ascribed to the oxidation state of the Ir. However, deconvolution of the Ir 4f region (Fig. 5c) and d)) shows only a marginally higher fraction of Ir^{4+} with respect to Ir^{3+} in unpolished (58.5%), compared to polished sensors (54.1%). Given that the IrOx film deposited on polished electrodes show a greater pH sensitivity, it is clear that factors other than the Ir oxidation

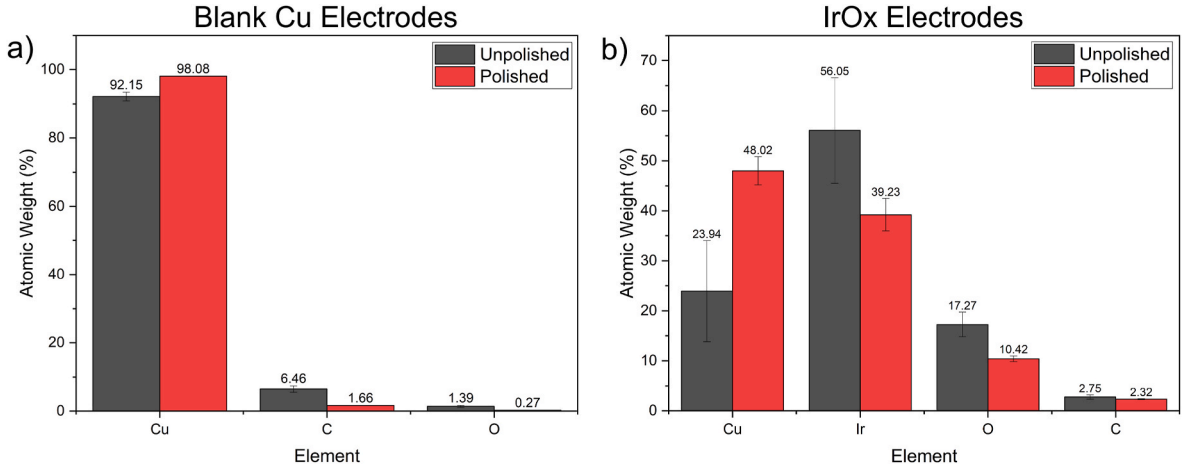

Fig. 4. a) Relative elemental composition of unpolished and polished Cu electrodes prior to IrOx deposition. The atomic weight % for each element was calculated from the average value across 3 scan regions and 2 samples of each type. Error bars correspond to the standard deviation. b) Relative elemental composition of IrOx film electrodeposited on unpolished and polished Cu electrodes.

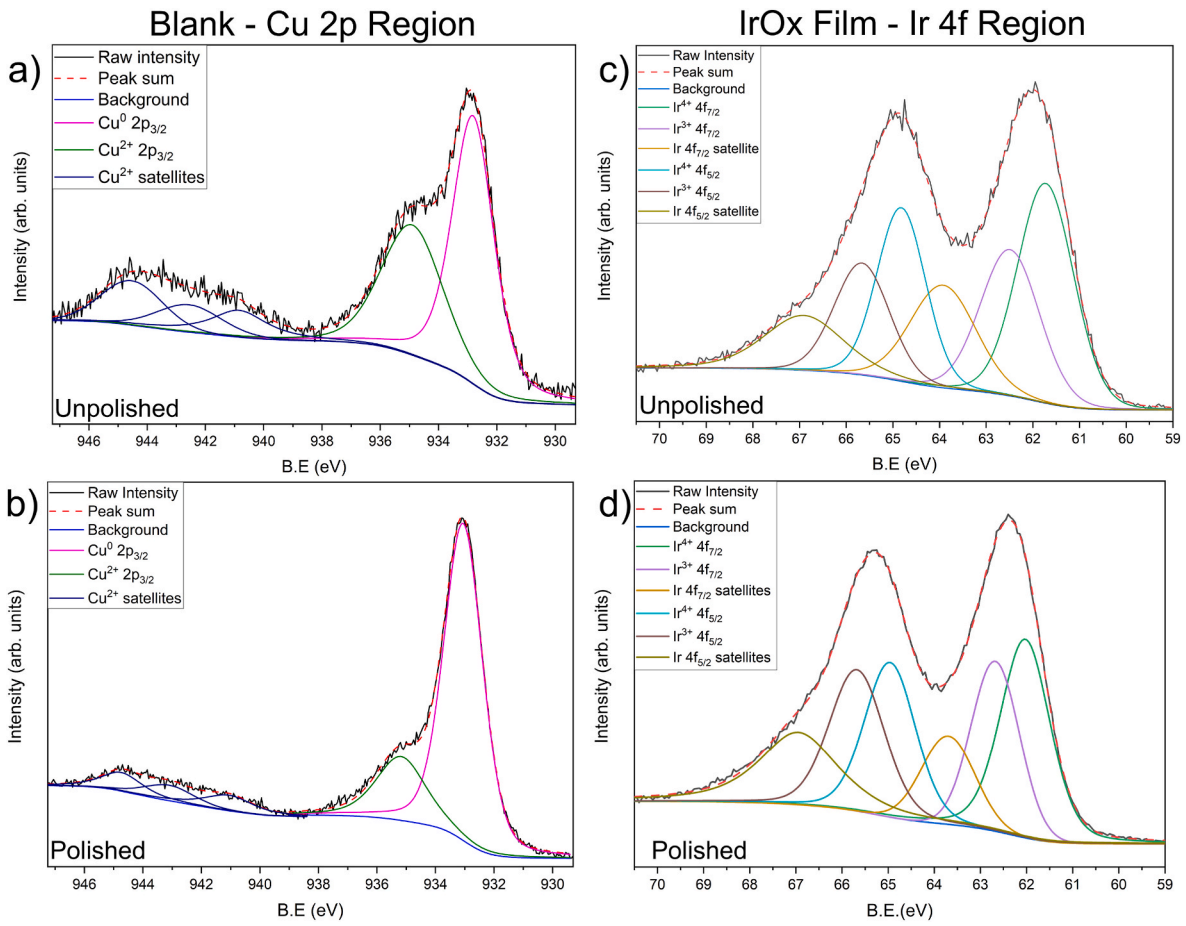

Fig. 5. Cu 2p region of a) unpolished and b) polished Cu electrodes prior to IrOx deposition. Deconvoluted Ir 4f region of IrOx film electrodeposited on c) unpolished and d) polished Cu electrodes. Here, the unpolished electrode displayed a pH sensitivity of 37.8 mV/pH while the polished sensor was measured to have a pH sensitivity of 73.2 mV/pH.

state dominate the observed improvement in pH sensitivity.

3.6. Discussion

From our comprehensive physical and chemical analysis, we conclude that the high median pH sensitivity and repeatability associated with IrOx films electrodeposited on polished Cu electrodes relates to the improved uniformity of the IrOx films. Specifically, localised regions of high oxide and carbonaceous contamination (as observed on unpolished electrodes) impede faradaic transport of electrons across the electrode-solution interface, leading to preferential formation of IrOx nanostructures (Fig. 3c)) rather than electrodeposition of a uniform film. These contaminants are removed effectively by electropolishing, as shown by both EDX (Fig. 4a) and XPS (Fig. 5a) and b)) chemical analysis, enabling electrodeposition of IrOx to occur more uniformly across the electrode surface (Fig. 3d)), although a reduced number of nanoparticle clusters are still observed.

In addition, the high surface roughness associated with the unpolished sensors (Fig. 3a)) would also lead to an electric field that varies locally at the surface, further reducing uniformity of the IrOx electrodeposition process. In contrast, the largely smooth copper surface following electropolishing of the Cu electrodes (Fig. 3b)) supports the growth of a more uniform IrOx film leading to the high reproducibility in pH sensitivity observed for polished sensors.

We note, while our analysis reveals the importance of IrOx uniformity, the redox activity of the Ir complexes within the hydrated IrOx film also influences the observed pH-sensitivity. Indeed, detailed analysis of deposition cyclic voltammograms for a range of dEGFETs assembled using IrOx films on polished Cu electrodes, reveals a direct correlation between the measured pH sensitivity and surface concentration of redox active Ir^{3+} complexes (SI S11)). These subtle differences explain the small device-to-device variability observed for polished Cu electrodes (±5 mV/pH) and this understanding could be used to further improve repeatability.

3.7. β-Lactamase dEGFET detection

Finally, we demonstrate our highly pH-sensitive, dEGFET PCB sensor to quantify the pH change resulting from an enzyme catalysed reaction. Specifically, we employed our sensors to quantify the pH change resulting from β-lactamase mediated hydrolysis of a β-lactam antibiotic (ampicillin). Additional details on the reaction and detection principle are presented in SI S12. Tests of this nature may ultimately find application in assessing antimicrobial susceptibility or for monitoring antibiotic concentrations in patient samples.

Fig. 6) shows the pH change occurring in a solution of ampicillin after 45 min incubation with a β-lactamase blend, where the ampicillin concentration varies between 0 and 200 μg/mL. SI S13 reports the same measurements where instead the raw dEGFET output voltage is presented without prior pH calibration, highlighting the high repeatability of device pH response. The limit of detection (LOD) was calculated as described in (Armbruster and Pry, 2008). Briefly, a limit of blank (LOB) was calculated using the mean and SD of blank samples (n = 4), LOB = $blank_{mean}$ + (1.645 × $blank_{SD}$). Subsequently the LOD was calculated using the SD at the lowest ampicillin concentration according to LOD = LOB + (1.645 × $lowampicillin_{SD}$). For this assay, the LOD was found to be

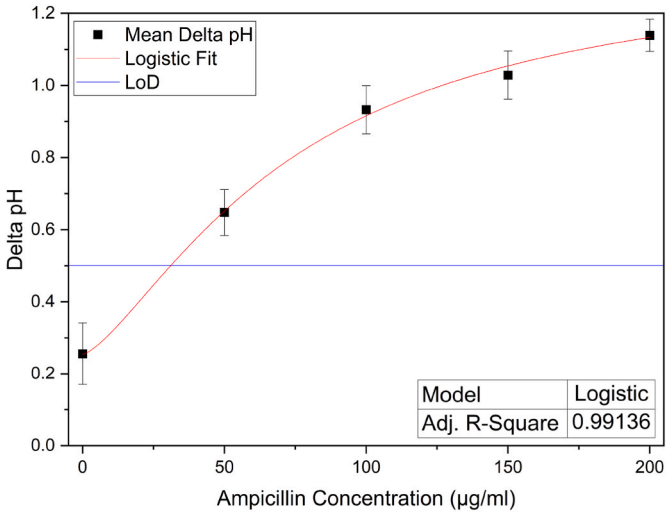

Fig. 6. Calibration curve showing the change in pH measured using dEGFET PCB sensors as a function of ampicillin concentration, 45 min after incubation in the β-lactamase enzyme containing solution. Horizontal line at 0.5 pH indicates the limit of detection (LOD). Error bars represent the standard deviation of repeat measurements.

31.0 μg/mL of ampicillin which compares well with levels of ampicillin found clinically in urine (ranging between 44.3 and 177.6 μg/mL (Meyers et al., 1991)).

4. Conclusion

We have demonstrated a low-cost and simple to manufacture pH sensor that comprises a discrete transistor, coupled to an extended gate Cu electrode manufactured on PCB that is rendered pH-sensitive through an electrodeposited IrOx film. In contrast to previous dEGFETs on PCB, our sensors displayed beyond-Nernstian pH responses with very low device-to-device variability. These excellent performance characteristics arise from the improved uniformity of the IrOx film achieved by electropolishing the Cu electrodes prior to IrOx deposition, which not only removes oxides and adventitious carbon contamination but also reduces the electrode surface roughness. Finally, we demonstrated that the sensor is capable of quantifying the concentration of a β-lactam antibiotic (ampicillin) through the pH change that occurs due to the action of a β-lactamase enzyme blend. This work showcases the potential of low-cost PCB dEGFET devices towards enzyme-catalysed reactions relevant across a range of global challenges.

CRediT authorship contribution statement

Rhys D. Ashton: Methodology, Investigation, Formal Analysis, Writing - Original Draft, Writing - Review and Editing. Callum D. Silver: Methodology, Validation, Writing - Review and Editing. TobyW. Bird: Investigation, Formal Analysis, Writing - Review and Editing. Ben Coulson: Investigation, Formal Analysis, Writing - Review and Editing. Andrew Pratt: Formal Analysis, Writing - Review and Editing, Supervision. Steven David Johnson: Conceptualization, Writing - Original Draft, Writing - Review and Editing, Supervision.

Declaration of competing interest

The authors declare that they have no known competing financial interests or personal relationships that could have appeared to influence the work reported in this paper.

Data availability

Data will be made available on request.

Acknowledgments

This work was supported by the EPSRC (grants EP/P027571/1 'Sensors for clean water: a participatory approach for technology innovation' and EP/P02324X/1 'Multiparameter Assay for Profiling Susceptibility [MAPS]').

Appendix A. Supplementary data

Supplementary data to this article can be found online at https://doi.org/10.1016/j.bios.2023.115150.

References

Anastasova, S., Kassanos, P., Yang, G.Z., 2018. Multi-parametric rigid and flexible, low-cost, disposable sensing platforms for biomedical applications. Biosens. Bioelectron. 102, 668–675. https://doi.org/10.1016/j.bios.2017.10.038.

Armbruster, D.A., Pry, T., 2008. Limit of blank, limit of detection and limit of quantitation. Clin. Biochem. Rev. 29 (Suppl. 1), S49–S52. https://www.ncbi.nlm.nih.gov/pmc/articles/PMC2556583.

Awad, A., Ghany, N.A., Dahy, T., 2010. Removal of tarnishing and roughness of copper surface by electropolishing treatment. Appl. Surf. Sci. 256, 4370–4375. https://doi.org/10.1016/j.apsusc.2010.02.033.

Bergveld, P., 2003. ISFET, theory and practice. In: IEEE Sensor Conference, pp. 1–26. Toronto. URL: https://www.idc-online.com/technical_references/pdfs/mechanical_engineering/ISFET-Bergveld.pdf.

Burke, L.D., Whelan, D.P., 1984. A voltammetric investigation of the charge storage reactions of hydrous iridium oxide layers. J. Electroanal. Chem. Interfacial Electrochem. 162, 121–141. https://doi.org/10.1016/S0022-0728(84)80159-X.

Chi, L.L., Chou, J.C., Chung, W.Y., Sun, T.P., Hsiung, S.K., 2000. Study on extended gate field effect transistor with tin oxide sensing membrane. Mater. Chem. Phys. 63, 19–23. https://doi.org/10.1016/S0254-0584(99)00184-4.

Cho, W.J., Lim, C.M., 2018. Sensing properties of separative paper-based extended-gate ion-sensitive field-effect transistor for cost effective pH sensor applications. Solid State Electron. 140, 96–99. https://doi.org/10.1016/j.sse.2017.10.025.

Elsen, H.A., Monson, C.F., Majda, M., 2009. Effects of electrodeposition conditions and protocol on the properties of iridium oxide pH sensor electrodes. J. Electrochem. Soc. 156, F1. https://doi.org/10.1149/1.3001924.

Freakley, S.J., Ruiz-Esquius, J., Morgan, D.J., 2017. The X-ray photoelectron spectra of Ir, IrO_2 and $IrCl_3$ revisited: the X-ray photoelectron spectra of Ir, IrO_2 and $IrCl_3$ revisited. Surf. Interface Anal. 49, 794–799. https://doi.org/10.1002/sia.6225.

Giri, S.D., Sarkar, A., 2016. Electrochemical study of bulk and monolayer copper in alkaline solution. J. Electrochem. Soc. 163, H252–H259. https://doi.org/10.1149/2.0071605jes.

Gowers, S.A.N., Freeman, D.M.E., Rawson, T.M., Rogers, M.L., Wilson, R.C., Holmes, A. H., Cass, A.E., O'Hare, D., 2019. Development of a minimally invasive microneedle-based sensor for continuous monitoring of β-lactam antibiotic concentrations in vivo. ACS Sens. 4, 1072–1080. https://doi.org/10.1021/acssensors.9b00288.

Hendrikse, J., Olthuis, W., Bergveld, P., 1997. A drift free nernstian iridium oxide pH sensor. In: Proceedings of International Solid State Sensors and Actuators Conference (Transducers '97). IEEE, Chicago, IL, USA, pp. 1367–1370. https://doi.org/10.1109/SENSOR.1997.635491.

Hillman, A.R., Skopek, M.A., Gurman, S.J., 2011. X-Ray spectroscopy of electrochemically deposited iridium oxide films: detection of multiple sites through structural disorder. Phys. Chem. Chem. Phys. 13, 5252–5263. https://doi.org/10.1039/C0CP01472A.

Hu, J., Abdelsalam, M., Bartlett, P., Cole, R., Sugawara, Y., Baumberg, J., Mahajan, S., Denuault, G., 2009. Electrodeposition of highly ordered macroporous iridium oxide through self-assembled colloidal templates. J. Mater. Chem. 19, 3855. https://doi.org/10.1039/b900279k.

Huang, W.D., Cao, H., Deb, S., Chiao, M., Chiao, J., 2011. A flexible pH sensor based on the iridium oxide sensing film. Sensor Actuator Phys. 169, 1–11. https://doi.org/10.1016/j.sna.2011.05.016.

Hung, S.C., Cheng, N.J., Yang, C.F., Lo, Y.P., 2014. Investigation of extended-gate field-effect transistor pH sensors based on different-temperature-annealed bi-layer MWCNTs-In2O3 films. Nanoscale Res. Lett. 9, 502. https://doi.org/10.1186/1556-276X-9-502.

Kaisti, M., Boeva, Z., Koskinen, J., Nieminen, S., Bobacka, J., Levon, K., 2016. Hand-held transistor based electrical and multiplexed chemical sensing system. ACS Sens. 1, 1423–1431. https://doi.org/10.1021/acssensors.6b00520.

Kim, T.Y., Yang, S., 2014. Fabrication method and characterization of electrodeposited and heat-treated iridium oxide films for pH sensing. Sensor. Actuator. B Chem. 196, 31–38. https://doi.org/10.1016/j.snb.2014.02.004.

Kim, Y.J., Lee, Y.C., Sohn, B.K., Lee, J.H., Kim, C.S., 2003. A novel pH microsensor with a built-in reference electrode. J. Kor. Phys. Soc. 43, 769. https://doi.org/10.3938/jkps.43.769.

Manjakkal, L., Szwagierczak, D., Dahiya, R., 2020. Metal oxides based electrochemical pH sensors: current progress and future perspectives. Prog. Mater. Sci. 109, 100635 https://doi.org/10.1016/j.pmatsci.2019.100635.

Marzouk, S.A.M., 2003. Improved electrodeposited iridium oxide pH sensor fabricated on etched titanium substrates. Anal. Chem. 75, 1258–1266. https://doi.org/10.1021/ac0261404.

Meyer, R., Cogan, S., Nguyen, T., Rauh, R., 2001. Electrodeposited iridium oxide for neural stimulation and recording electrodes. IEEE Trans. Neural Syst. Rehabil. Eng. 9, 2–11. https://doi.org/10.1109/7333.918271.

Meyers, B.R., Wilkinson, P., Mendelson, M.H., Walsh, S., Bournazos, C., Hirschman, S.Z., 1991. Pharmacokinetics of ampicillin-sulbactam in healthy elderly and young volunteers. Antimicrob. Agents Chemother. 35, 2098–2101. https://doi.org/10.1128/AAC.35.10.2098.

Moschou, D., Trantidou, T., Regoutz, A., Carta, D., Morgan, H., Prodromakis, T., 2015. Surface and electrical characterization of Ag/AgCl pseudo-reference electrodes manufactured with commercially available PCB technologies. Sensors 15, 18102–18113. https://doi.org/10.3390/s150818102.

Naseer, A., Khan, A.Y., 2009. A study of growth and breakdown of passive film on copper surface by electrochemical impedance spectroscopy. Turk. J. Chem. https://doi.org/10.3906/kim-0708-23.

National Institute of Standards and Technology, 2000. X-Ray photoelectron spectroscopy database XPS,version 4.1. NIST Standard Reference Database 20. https://doi.org/10.18434/T4T88K.

Olthuis, W., Robben, M., Bergveld, P., Bos, M., van der Linden, W., 1990. pH sensor properties of electrochemically grown iridium oxide. Sensor. Actuator. B Chem. 2, 247–256. https://doi.org/10.1016/0925-4005(90)80150-X.

Otsu, N., 1979. A threshold selection method from gray-level histograms. IEEE Transactions on Systems, Man, and Cybernetics 9, 62–66. https://doi.org/10.1109/TSMC.1979.4310076.

Pfeifer, V., Jones, T.E., Velasco Vélez, J.J., Massué, C., Arrigo, R., Teschner, D., Girgsdies, F., Scherzer, M., Greiner, M.T., Allan, J., Hashagen, M., Weinberg, G., Piccinin, S., Hävecker, M., Knop-Gericke, A., Schlögl, R., 2016. The electronic structure of iridium and its oxides: the electronic structure of iridium and its oxides. Surf. Interface Anal. 48, 261–273. https://doi.org/10.1002/sia.5895.

Prodromakis, T., Liu, Y., Toumazou, C., 2011a. A low-cost disposable chemical sensing platform based on discrete components. IEEE Electron. Device Lett. 32, 417–419. https://doi.org/10.1109/LED.2010.2099098.

Prodromakis, T., Liu, Y., Yang, J., Hollinghurst, D., Toumazou, C., 2011b. A novel design approach for developing chemical sensing platforms using inexpensive technologies. In: 2011 IEEE Biomedical Circuits and Systems Conference (BioCAS). IEEE, San Diego, CA, USA, pp. 369–372. https://doi.org/10.1109/BioCAS.2011.6107804.

Rothberg, J.M., Hinz, W., Rearick, T.M., Schultz, J., Mileski, W., Davey, M., Leamon, J. H., Johnson, K., Milgrew, M.J., Edwards, M., Hoon, J., Simons, J.F., Marran, D., Myers, J.W., Davidson, J.F., Branting, A., Nobile, J.R., Puc, B.P., Light, D., Clark, T. A., Huber, M., Branciforte, J.T., Stoner, I.B., Cawley, S.E., Lyons, M., Fu, Y., Homer, N., Sedova, M., Miao, X., Reed, B., Sabina, J., Feierstein, E., Schorn, M., Alanjary, M., Dimalanta, E., Dressman, D., Kasinskas, R., Sokolsky, T., Fidanza, J.A., Namsaraev, E., McKernan, K.J., Williams, A., Roth, G.T., Bustillo, J., 2011. An integrated semiconductor device enabling non-optical genome sequencing. Nature 475, 348–352. https://doi.org/10.1038/nature10242.

Salm, E., Zhong, Y., Reddy, B., Duarte-Guevara, C., Swaminathan, V., Liu, Y.S., Bashir, R., 2014. Electrical detection of nucleic acid amplification using an on-chip quasi-reference electrode and a PVC REFET. Anal. Chem. 86, 6968–6975. https://doi.org/10.1021/ac500897t.

Shaikh, A.A., Firdaws, J., Serajee, S., Rahman, M.S., Bakshi, P.K., 2011. Electrochemical studies of the pH dependence of Cu(II) reduction in aqueous britton-robinson buffer solution. Int. J. Electrochem. Sci. 6, 11. URL: http://www.electrochemsci.org/papers/vol6/6072333.pdf.

Steegstra, P., Ahlberg, E., 2012. Influence of oxidation state on the pH dependence of hydrous iridium oxide films. Electrochim. Acta 76, 26–33. https://doi.org/10.1016/j.electacta.2012.04.143.

Steegstra, P., Busch, M., Panas, I., Ahlberg, E., 2013. Revisiting the redox properties of hydrous iridium oxide films in the context of oxygen evolution. J. Phys. Chem. C 117, 20975–20981. https://doi.org/10.1021/jp407030r.

Toumazou, C., Shepherd, L.M., Reed, S.C., Chen, G.I., Patel, A., Garner, D.M., Wang, C.J. A., Ou, C.P., Amin-Desai, K., Athanasiou, P., Bai, H., Brizido, I.M.Q., Caldwell, B., Coomber-Alford, D., Georgiou, P., Jordan, K.S., Joyce, J.C., La Mura, M., Morley, D., Sathyavruthan, S., Temelso, S., Thomas, R.E., Zhang, L., 2013. Simultaneous DNA amplification and detection using a pH-sensing semiconductor system. Nat. Methods 10, 641–646. https://doi.org/10.1038/nmeth.2520.

Trantidou, T., Payne, D.J., Tsiligkiridis, V., Chang, Y.C., Toumazou, C., Prodromakis, T., 2013. The dual role of Parylene C in chemical sensing: acting as an encapsulant and as a sensing membrane for pH monitoring applications. Sensor. Actuator. B Chem. 186, 1–8. https://doi.org/10.1016/j.snb.2013.05.077.

Wagner, C.D., Davis, L.E., Zeller, M.V., Taylor, J.A., Raymond, R.H., Gale, L.H., 1981. Empirical atomic sensitivity factors for quantitative analysis by electron spectroscopy for chemical analysis. Surf. Interface Anal. 3, 211–225. https://doi.org/10.1002/sia.740030506.

Yamanaka, K., 1989. Anodically electrodeposited iridium oxide films (AEIROF) from alkaline solutions for electrochromic display devices. Jpn. J. Appl. Phys. 28, 632–637. https://doi.org/10.1143/JJAP.28.632.

Yang, T.H., Chang, S.P., Li, C.W., Chang, S.J., 2012. Sensing performance of EGFET pH sensors with CuO nanowires fabricated on glass substrate. ECS Meeting Abstracts MA2012–02. https://doi.org/10.1149/MA2012-02/35/2770, 2770–2770.

Yates, D.E., Levine, S., Healy, T.W., 1974. Site-binding model of the electrical double layer at the oxide/water interface. J. Chem. Soc., Faraday Trans. 70, 1807. https://doi.org/10.1039/f19747001807, 1: Physical Chemistry in Condensed Phases.

Yin, L.T., Chou, J.C., Chung, W.Y., Sun, T.P., Hsiung, S.K., 2000. Separate structure extended gate H+-ion sensitive field effect transistor on a glass substrate. Sensor. Actuator. B Chem. 71, 106–111. https://doi.org/10.1016/S0925-4005(00)00613-4.

Zaman, S., Asif, M., Zainelabdin, A., Amin, G., Nur, O., Willander, M., 2011. CuO nanoflowers as an electrochemical pH sensor and the effect of pH on the growth. J. Electroanal. Chem. 662, 421–425. https://doi.org/10.1016/j.jelechem.2011.09.015.

Zea, M., Moya, A., Fritsch, M., Ramon, E., Villa, R., Gabriel, G., 2019. Enhanced performance stability of iridium oxide-based pH sensors fabricated on rough inkjet-printed platinum. ACS Appl. Mater. Interfaces 11, 15160–15169. https://doi.org/10.1021/acsami.9b03085.